Thermal transport measurements in six-beam, ultraviolet irradiation of spherical targets

B. Yaakobi, O. Barnouin, J. Delettrez, L. M. Goldman, R. Marjoribanks, R. L. McCrory, M. C. Richardson, and J. M. Soures
Laboratory for Laser Energetics, 250 East River Road, University of Rochester, Rochester, New York 14623

(Received 15 October 1984; accepted for publication 7 December 1984)

Thermal transport, mass ablation rates, and preheat have been studied in spherical irradiation at $\lambda = 351$ nm, using six of the 24 beams of the OMEGA spherical irradiation laser system at the Laboratory for Laser Energetics. Mass ablation rates are higher at 351-nm than at 1054-nm irradiation, even when compared at the same absorbed irradiance. Similar to the case of 1054-nm irradiation, very deep burnthrough was found at 351 nm. However, the shallow-gradient temperature profile at the heat front, characteristic of the experiments at 1054 nm, was not observed here, nor was the large difference between uniform and tight focus irradiation of spherical targets. Ablation pressures derived from charge-collector data rise from 10 to 100 Mbar for absorbed irradiance in the range of 4×10^{13} to 9×10^{14} W/cm^2.

I. INTRODUCTION

Thermal transport in laser-target interaction is an important process determining the ablation pressure and the hydrodynamic efficiency.[1] Recent experiments at $\lambda = 1054$ nm at the Rutherford Laboratory[2] and at the Laboratory for Laser Energetics[3] (LLE) have shown that the heat fluxes are higher in spherical irradiation than in planar-target irradiation. Planar-target, single-beam irradiation could be described in terms of flux inhibition with a limiter of about $f = 0.03$, even for $\lambda = 351$ nm irradiation.[4] The experiments at the Rutherford Laboratory[2] involving spherical, $\lambda = 1054$ nm irradiation could be described essentially by uninhibited transport ($f \gtrsim 0.1$). Similar experiments at LLE showed[3] that the heat front is characterized by a much smaller temperature gradient than predicted by a flux-limited model at any value of f. Additionally, part of the very deep heat penetration may have a similar effect to that of preheat rather than contribute to ablation. These effects were thought to be due to noncollisional effects, i.e., due to electrons of long mean free path on the tail of the thermal distribution of velocities.[5] It is therefore interesting and important to conduct transport experiments in spherical illumination at $\lambda = 351$ nm. The results below show that thermal transport in spherical, 351-nm irradiation is similar to that at 1054-nm irradiation only in that the penetration depth is much higher than predicted by a flux-limited model. However, the sharp difference between burnthrough measurements with various substrate materials or between uniform and tight-focus irradiation on spherical targets found in the 1054-nm experiments[3] were not found in the present measurements. One expects that noncollisional effects will be reduced at short-wavelength irradiation, because of the higher plasma density at which the laser is absorbed. The present results are consistent with these expectations.

II. TRANSPORT EXPERIMENTS

The targets in these experiments were solid plastic spheres coated with a signature layer (aluminum or titanium) of thickness 3 μm, overcoated with parylene layers of different thicknesses. The size of the target was adjusted to yield irradiances in the range 10^{14}–10^{15} W/cm^2. Because solid targets do not implode, transport issues can be studied without the interference of implosion phenomena. The laser consisted of six of the 24 beams of the OMEGA laser system,[6] frequency tripled using a scheme[7] developed at LLE. Pulses were of 600 ps full width at half maximum (FWHM) and energy in the range 150–235 J. The major diagnostics used in these experiments were time-integrating x-ray crystal spectrographs, an x-ray streak camera with a filter array for energy selection, charged-particle detectors (Faraday cups), and plasma calorimeters for measuring the absorbed energy.

Figure 1 shows the results obtained with six-blue-beam irradiation ($\lambda = 351$ nm) of plastic (CH)-coated targets with an aluminum signature layer. The ordinate is the relative intensity of the Lyman-α line of Al^{+12} at 1.728 keV and the abscissa is the CH thickness. We refer to such plots as "burnthrough curves." Strictly speaking, the appearance of x-ray lines is indicative of ionization and excitation, whereas their interpretation in terms of a local temperature precludes nonlocal effects, e.g., those due to electrons or radiation flowing from the hot interaction region. The burnthrough penetration is considerably deeper than predicted by a flux-limited model, as was found for 1054-nm irradiation.[3] We use the 500-eV electron temperature contour for the definition of burnthrough, but the conclusions are very insensitive to this choice because of the steepness of the calculated profile. The theoretical results are shown by the hatched bands in Fig. 1, where for each of three irradiance values and for f values in the range 0.04–0.1, the LILAC code[8] was used to calculate the Al^{+12} resonance line intensity as a function of the CH-coating thickness. Each experimental or theoretical curve is separately normalized to 1 at zero CH thickness. The numerical replication of the *shape* of the burnthrough curves is much less sensitive to the details of the atomic physics than that of the absolute intensity of the radiation. In each band the left boundary corresponds to $f = 0.04$, whereas the right boundary corresponds to $f = 0.1$. At an irradiance of 10^{14} W/cm^2, the band is very narrow and is represented by a single curve.

 0021-8979/85/094354-06$02.40

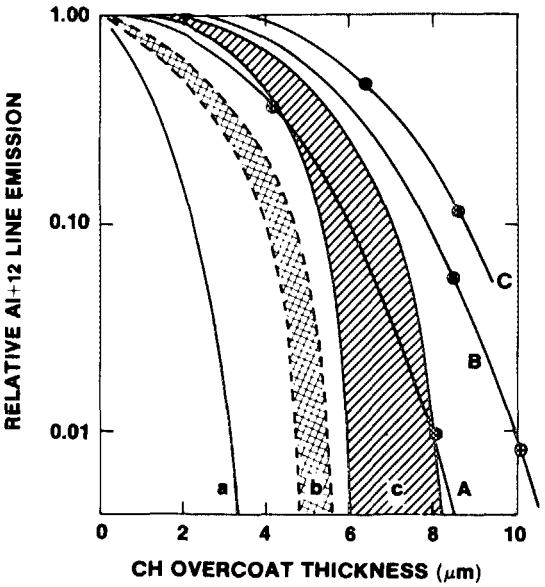

FIG. 1. Experimental burnthrough curves: intensity of the Lyman-α line of Al^{+12} from an aluminum substrate as a function of the CH-overcoat-layer thickness. Irradiance (in W/cm^2): A–10^{14}, B–5×10^{14}, C–10^{15}. Theoretical curves are shown in hatched bands where the left boundary corresponds to a flux limiter $f=0.04$ and the right boundary to $f=0.1$. Theoretical bands a, b, c are for the same irradiances as A, B, C, respectively.

The three experimental curves correspond to the same three irradiance values (in W/cm^2) as those of the theoretical curves: 10^{14} (A), 5×10^{14} (B), and 10^{15} (C). Penetration larger than predicted is a common feature of the measurements at 1054 nm as well as at 351 nm. However, at $\lambda=1054$ nm we measured penetration which is deeper than that predicted by about a factor 3, for any irradiance in the range 5×10^{13}–10^{15} W/cm^2. In comparison, at $\lambda=351$ nm this factor decreases from ~3 at 10^{14} W/cm^2 to ~2 at 5×10^{14} W/cm^2, and finally to ~1.5 at 10^{15} W/cm^2. In these comparisons the code calculations refer to CH-coated aluminum. The calculated absorbed energy agreed with the measurements for small f values ($f=0.04$–0.06), but for $f=0.1$ the absorption by inverse bremsstrahlung had to be reduced by about a factor of 2 to maintain this agreement.

Earlier transport measurements[3] at $\lambda=1054$ nm showed a substantial disparity between uniform and tight-focus irradiation, and it is therefore of interest to make a similar comparison with the present, UV irradiation. Figures 2 and 3 show x-ray microscope images of targets with aluminum substrates and CH overcoats of various thicknesses. These images show deep heat-front penetration in both irradiation geometries. The peak-to-valley variation along the ring in shot 9418 is 50%, but this increases to a factor of 5 in shot 9415 because of a slight beam imbalance. The energy of the laser was adjusted to yield an irradiance of about 5×10^{14} W/cm^2 in all shots of Figs. 2 and 3.

We next show in Fig. 4 the results of burnthrough measurements with aluminum substrates for three different focusing conditions: (a) uniform illumination achieved by focusing eight target radii behind the center of the target, thereby overlapping the beams; (b) contiguous focusing, where the beams almost completely cover the target surface without overlap; and (c) tight focus, where the beam imprint on the target surface (35 μm diam) is much smaller than the distance between adjacent beams. In all three cases, the beam energies were adjusted to yield approximately the same irradiance: 5×10^{14} W/cm^2. As seen, the results do not show the wide disparity between the various focusing conditions that was observed for 1054-nm irradiation (Ref. 3, Fig. 6); this phenomena can be attributed to the higher collisionality with 351-nm irradiation. The mean free path (MFP) of a typical electron is significantly shorter in 351-nm as compared to 1054-nm irradiation; this is because of the higher density, as well as the lower temperature (if comparison is made on the basis of absorbed energy) in the former case. Lateral effects responsible for the dependence on the focusing conditions can be expected to involve electrons of long MFP. For short-wavelength irradiation there will be a much smaller fraction of the velocity distribution for which the MFP is longer than the tight focal spot diameter. However, the difference between the flat-target, single-beam results obtained with the glass development laser[9] (GDL) (Ref. 4, Fig. 1) and the tight-focus results in Fig. 4 are still puzzling. Both cases entail 351-nm irradiation, but whereas the GDL results can be modeled with $f=0.04$ flux inhibition, those of Fig. 4 indicate uninhibited transport. We tentatively attribute this difference to either the difference in the focusing conditions ($f/3$ on OMEGA, $f/13$ on GDL) or to differences in beam quality. A lower beam quality in GDL could reduce radial heat transport via generation of magnetic fields.

In Fig. 5 we show burnthrough curves obtained by measuring various x-ray lines from titanium substrates. The lines are $1s^2$-$1s2p$ transition of Ti^{+20} at 4.73 keV, the $1s^2$-$1s3p$ transition of Ti^{+20} at 5.56 keV, and the $2s$-$4p$ transition of

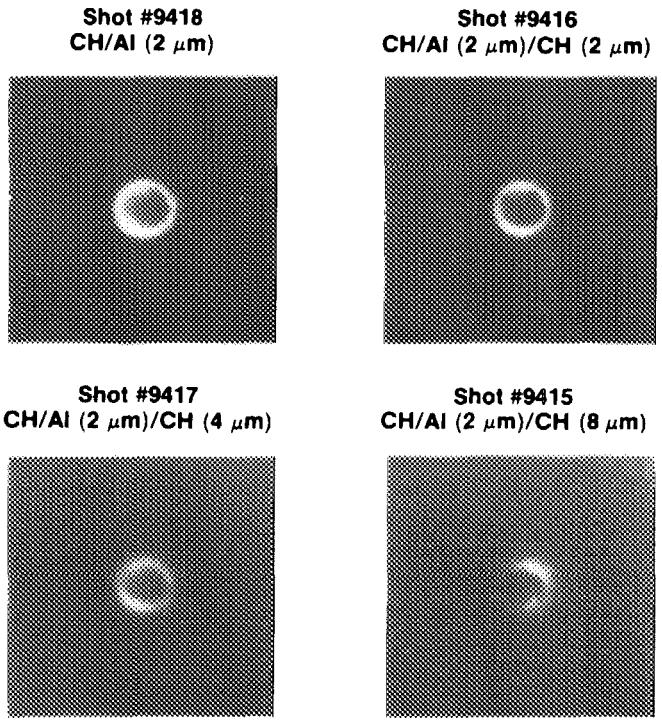

FIG. 2. X-ray microscope images (around 3 keV) of targets irradiated uniformly at 5×10^{14} W/cm^2. Targets are CH solid spheres coated with 2 μm of aluminum, and then with CH of various thicknesses.

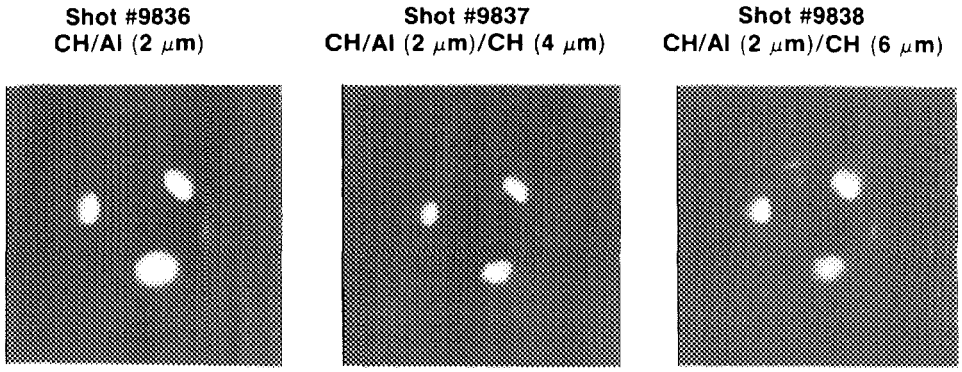

FIG. 3. X-ray microscope images (0.8–2.2 keV) of targets irradiated with 45-μm-diam spots, at 5×10^{14} W/cm^2. Only three of the six beam traces can be seen from any direction.

Ti^{+19}. In spite of the large disparity of energy between the Ti^{+19} and Ti^{+20} lines (indicating different probed temperatures), the curves are essentially identical. Also, the titanium curves (Fig. 5) and the aluminum curves (Fig. 4) are almost identical, in contradistinction to the results with 1054-nm irradiation (Ref. 3, Figs. 7 and 8). Again, the results with 351-nm irradiation are what one might expect for the higher collisionality of shorter-wavelength interaction. Because the temperature scale length is related to a typical MFP, which is much shorter for short-wavelength irradiation, the differences between the titanium and aluminum curves apparently become too small to resolve.

III. MASS ABLATION AND ABLATION PRESSURE

The burnthrough measurements can be used to estimate the peak mass ablation rate $\dot{m}$ and the ablation pressure P, if we assume that all the mass contributing to the measured line intensity is in fact heated and ablated. These quantities can alternatively be derived from charge-collector data and these indicate that this assumption may be incorrect. Figure 6 shows values of $\dot{m}$ derived from Fig. 4 juxtaposed against our previous $\dot{m}$ data.[3] The mass ablation rate is obtained from the total ablated mass Δm, conservatively taken as the mass of that CH thickness which corresponds to an aluminum radiation drop by a factor of 10. The peak mass ablation rate is then given by $\dot{m} = \alpha \Delta M/\tau$, where τ is the pulse duration (FWHM) and α is a correction factor[2] (whose value is about 0.7), which accounts for the fact that the dependence of $\dot{m}$ on the laser intensity within one pulse is weaker than linear.

As argued in relation to the previous 1054-nm data,[3] the aluminum spectroscopic data may overestimate the mass ablation rate. However, in Fig. 6, $\dot{m}$ measured in the same way is seen to be higher for blue irradiation than for red irradiation. It should be noted that this advantage for laser fusion is in addition to that of higher absorption with the shorter-wavelength irradiation (since the results are plotted against the absorbed irradiance).

The mass ablation rate derived from the charged particle detectors is based on the equation $\dot{m} = 2\alpha E_a/4\pi R^2 \tau V^2$. Here E_a is the total absorbed energy and R is the radius of the ablation surface which for the nonimploding targets used here can be taken as the initial target radius; V is the asymptotic plasma expansion velocity. To the extent that the measured velocity distribution is sufficiently narrow, the charge state of the plasma ion need not be known. In these experiments, typically $\Delta V/V \sim 0.6$, where ΔV is the FWHM of the velocity distribution and V the velocity of the peak of the current. We have introduced a correction due to the finite spread of velocities. In this case, the average of V^2 over the

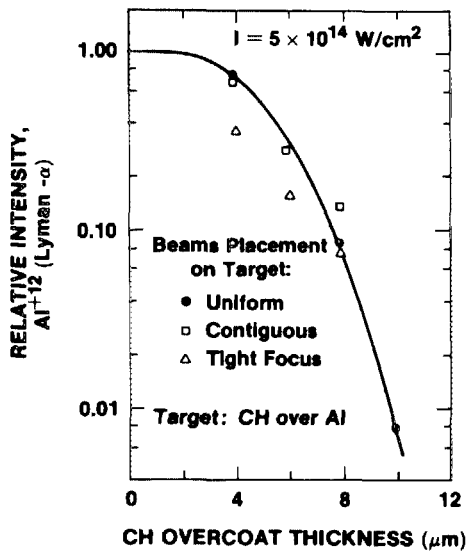

FIG. 4. Burnthrough curves for CH over aluminum targets for various focusing geometries.

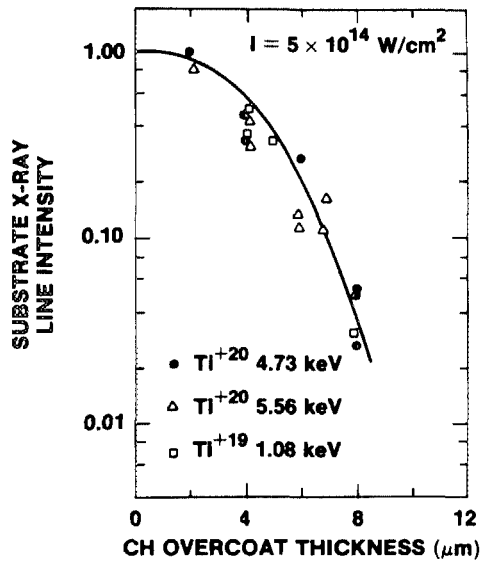

FIG. 5. Burnthrough curves for CH over titanium targets for different x-ray lines.

distribution is calculated from the data and the corresponding average velocity $(<V^2>)^{1/2}$ is smaller than the velocity of the peak by about 10%. This is because the current signal of the charge collectors, as a function of time, rises much faster than it falls. Additionally, the charge state of the ions, which is not known, was assumed here to be constant over the time when the current is significant. Since the charge state actually decreases for ions which arrive later, the correct average velocity should be somewhat lower. Thus the mass ablation rate determined from charge collectors should be viewed as a lower bound.

We compare in Fig. 6 the results thus obtained with previous data from 1054-nm irradiation along with the results obtained from the aluminum spectroscopic data. We see that when results obtained in the same way are compared, 351-nm irradiation outperforms 1054-nm irradiation even if the comparison is made on the basis of the same absorbed irradiance. The difference between $\dot{m}$ obtained with the two diagnostic methods on the same experiment can be the result of two effects: (a) the charge collectors underestimate the mass ablation rate because of neglecting the variation of charge state of the expanding ions, (b) the emission of aluminum lines (or other low-energy lines like those of Ti^{+19}) corresponds to material ahead of the ablation surface which is preheated due to nonlocal thermal transport; therefore, $\dot{m}$ is overestimated if derived from such measurements. Further studies are required to clarify these points. The mass ablation rate for 351-nm irradiation deduced from charge collectors follows the scaling law $\dot{m} = 3.8\times 10^5 (I/10^{14})^{0.53}$.

The plasma expansion velocity is lower at 351-nm than at 1054-nm irradiation for the same absorbed irradiance leading to a mass ablation rate which is higher for UV than for IR illumination at the same absorbed energy. The lower velocity is a result of the fact that a given amount of energy absorbed at a higher density for 351-nm irradiation leads to a lower temperature. The variation of the velocity with irradiance as demonstrated in Fig. 7 is weak in both cases and follows the scaling laws $V_p = 5.5\times 10^5 I^{0.15}$ for $\lambda = 1054$ nm and $V_p = 7.9\times 10^5 I^{0.15}$ for $\lambda = 351$ nm. Here V_p is the velocity (in cm/s) of the peak in the current distribution at an irradiance I (in W/cm^2).

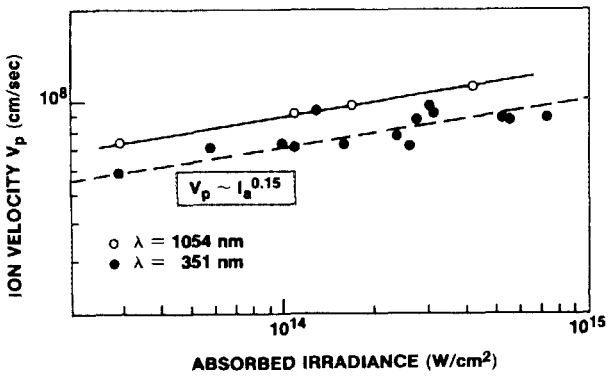

FIG. 7. Plasma expansion velocity (corresponding to the peak in the charge collector signals) at two irradiation wavelengths. The straight lines are fits to the experimental data.

In addition to time-integrated x-ray measurements described above, preliminary measurements of the time-dependence of x-ray emission in these experiments were made by a streak camera.[10] Typical results of the emission from titanium signature layers are shown in Fig. 8; these data were produced using a 1000-Å CsI photocathode deposited on a 25-μm beryllium substrate, with no direct laser fiducial. As is seen in this figure, the rise in x-ray emission, due to the heat front penetrating into the high-Z substrate, is progressively delayed by the addition of thicker CH overcoatings. Mass ablation rates are estimated from such data by dividing the mass density of the CH thickness corresponding to the relative time of burnthrough measured at some arbitrary emission level; presumably this emission level from identical signature layers in different targets roughly reflects a temperature level in the advancing heat front. Thus, the progress in time of some temperature contour in the heat front is charted. The data in Fig. 8 indicate an average burnthrough

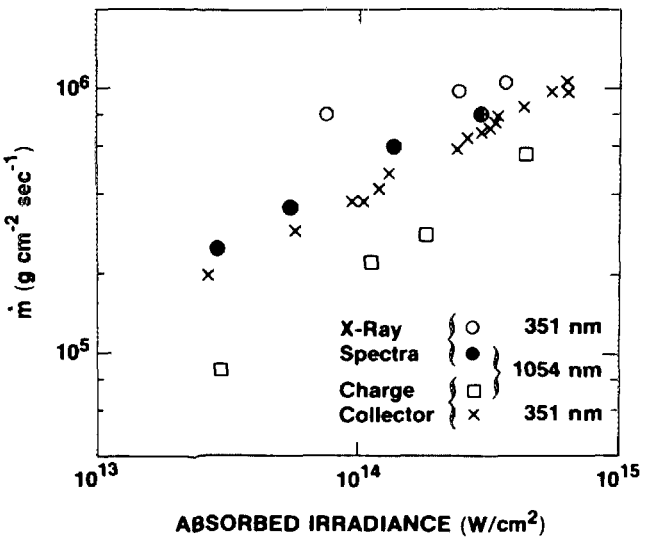

FIG. 6. Mass ablation rate estimated from burnthrough into an aluminum substrate (labeled "x-ray spectra") and from charge collectors, for both 351-nm and 1054-nm (from Ref. 3) irradiations.

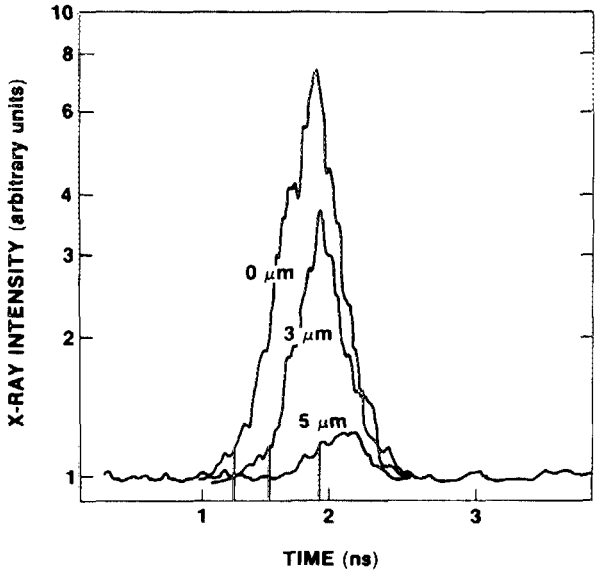

FIG. 8. X-ray streak camera measurements. Targets: CH solid spheres coated with 2 μm of titanium, then with CH of various thicknesses. Laser intensity 2×10^{14} W/cm^2. Peak of laser pulse approximately coincides with the peak of the emission curve for uncoated titanium.

rate of 5–6 μm per ns or an ablation rate of roughly $5–6\times10^5$ g cm^{-2} s^{-1}. Changes in the shape and magnitude of the time-resolved emission indicate that the front remains relatively steep during the laser pulse but decays and relaxes at later times, apparently after the peak of the laser pulse. These data do not provide sufficient resolution to infer the time-dependent mass ablation rate during the laser pulse. The time-resolved data are in general agreement with the time-integrated data of Figs. 1 and 4–6. First, data like those of Fig. 8 show larger burnthrough depths than predicted by flux-limited code calculations. Second, Al as compared with Ti substrates show similar behavior, as was observed with the time-integrated data. Finally, the mass ablation rates deduced here are very similar to those derived from time-integrated spectra (Fig. 6). For example, at an incident irradiance of 2×10^{14} W/cm^2, $\dot{m}$ derived from time-integrated results (Fig. 6, open circles) is 8×10^5 g cm^{-2} s^{-1}, as compared with $5–6\times10^5$ g cm^{-2} s^{-1} from Fig. 8.

The ablation pressure can be deduced from the mass ablation rate through the equation $P = c\dot{m}V$. Here c is a correction factor which was determined from code calculations to be about 0.7. This correction factor relates the charge collector measurements which take place long after the laser irradiation to the actual peak pressure during the laser pulse. If the code's description of transport is inaccurate, the calculated ablation pressure will be incorrect, but the *relationship* between the actual pressure and that calculated as $\dot{m}V$ can be expected to be essentially the same, except for a small modification of the correction factor c.

In Fig. 9, we compare the values of ablation pressure derived from the charge-collector data and the peak pressures calculated by LILAC for two values of f: 0.04 and 0.1. The experimental results are consistent with either calculated curve. This is equivalent to saying that $\dot{m}$ derived from charge collectors agrees with code predictions. However, Fig. 9 demonstrates clearly that pressure or mass ablation curves cannot be reliably used to deduce the value of f because P is little dependent on f when plotted against absorbed irradiance. Alternatively stated, the effect of transport on target dynamics is largely included in its effect on absorption. Burnthrough curves, however, are more suitable for studying transport directly, at least at high irradiances. This is because even large errors in the measured intensity will not displace the curves, such as those in Fig. 1, to a significantly different penetration depth.

IV. PREHEAT

We finally turn to the question of preheat in 351-nm irradiation, as measured by Ti-K_α lines. Using the same method in 1054-nm spherical irradiation on OMEGA we found that for increasing CH-overcoat thickness, the intensity of Ti^{+20} lines decreased very sharply, whereas the intensity of the K_α line decreased much more slowly [see Ref. 3, Fig. 9(a)]. This is simply because the K_α line is excited by fast electrons which move ahead of the heat front. This kind of behavior indicates that the range of the fast electrons is greater than the thickness of the heat-front region. By comparison, similar results for UV irradiation in the present experiments (Fig. 10) show the K_α line to decrease at the same

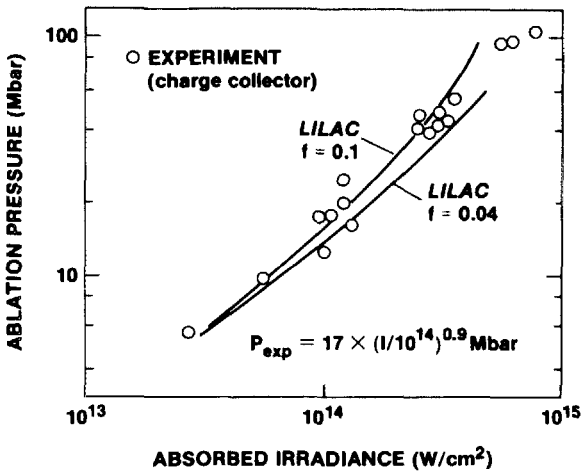

FIG. 9. Peak ablation pressure derived from charge collector data and from LILAC code calculations.

rate as that of Ti^{+20} lines. This indicates that the K_α line is excited by radiative preheat, rather than by fast electrons. Even though the resonance lines of Ti^{+20} are below the energy threshold for photoionizing neutral titanium atoms, their intensity is indicative of that of higher-energy lines and free-bound continuum which can photoionize titanium atoms.

If we assumed the K_α line to be excited by fast electrons, their range and therefore average energy could be determined from the plot of the measured K_α intensity as a function of CH-coating thickness. Such analysis using the present results (see Fig. 11) yields a hot-electron temperature of 3 keV. This temperature is about equal to the predicted thermal temperature for typical conditions in these experiments. Under these circumstances, these "fast" electrons would not efficiently excite K_α lines because their short range will not permit them to travel into the cold material ahead of the heat front. An objection to these deductions may be raised because the laser in the two experiments of Fig. 10 interacts, respectively, with different target materials: titanium and plastic. However, the interaction in these two cases is not very different. Measurements[11] showed that the laser absorption in titanium is only slightly higher than that in plastic at 5×10^{14} W/cm^2. Furthermore, the fast-electron temperature due to resonance absorption is a weak function of

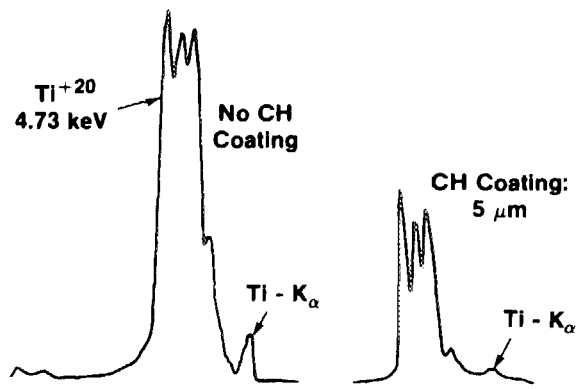

FIG. 10. Titanium plasma lines and K_α line for bare and CH-coated targets. Both spectra have the same vertical scale.

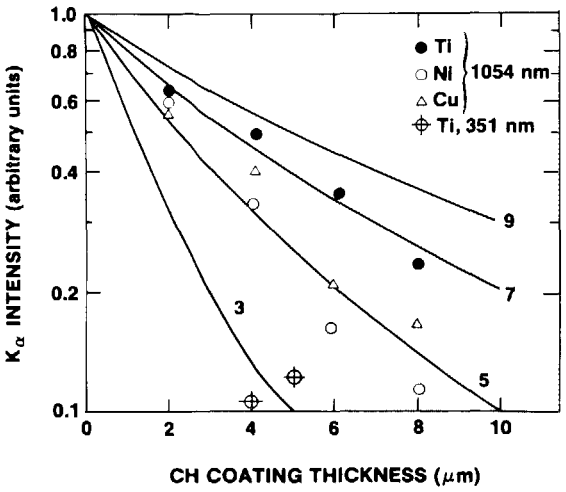

FIG. 11. K_α measurement of fast-electron temperature at 5×10^{14} W/cm^2. Experimental results at $\lambda = 1054$ nm irradiation are shown for comparison to the present, $\lambda = 351$ nm results with a titanium substrate. The solid lines are calculated by transporting electrons of the temperature shown near each curve (in keV), through the CH thickness shown on the abscissa. The intensity of K_α is normalized to that for zero CH thickness.

the nuclear charge Z. Of course, these difficulties inevitably arise when trying to determine preheat under conditions where it is essentially insignificant.

For sufficiently thick plastic coating, the intensity of the K_α line becomes immeasurably small. For 1054-nm irradiation, this simply means that the plastic prevents the fast electrons from reaching the titanium substrate, but preheat as such remains the same. However, the radiative preheat at 351-nm irradiation itself becomes negligibly small for plastic-coated targets.

V. CONCLUSION

The present results cannot be directly compared with results from other laboratories,[2,12] which were performed at different laser wavelengths (1054 and 527 nm). Some of these results[2] show an almost classical transport (e.g., a flux limiter $f \gtrsim 0.1$), as measured with both time-resolved spectroscopy and charge collectors. However, the large heat penetration obtained here with time-integrated as well as time-resolved spectral measurements was not observed elsewhere, nor was the discrepancy between spectral and charge-collector measurements. These differences can be due to differences in focusing optics, irradiation uniformity, or target size. Additionally, time-integrated x-ray measurements were not performed in the other studies, so a complete comparison is difficult to make.

In addition to further studying the issues mentioned above, measurements on the symmetric target implosion at short-wavelength irradiation should shed more light on the correct formulation of heat transport.

ACKNOWLEDGMENTS

This work was supported by the U. S. Department of Energy Office of Inertial Fusion under Contract No. DE-AC08-80DP40124 and by the Laser Fusion Feasibility Project at the Laboratory for Laser Energetics which has the following sponsors: Empire State Electric Energy Research Corporation, General Electric Company, New York State Energy Research and Development Authority, Northeast Utilities Service Company, Southern California Edison Company, The Standard Oil Company (Ohio), the University of Rochester. Such support does not imply endorsement of the content by any of the above parties.

Important contributions by R. S. Craxton, S. Skupsky, R. Epstein, and P. Jaanimagi are gratefully acknowledged.

[1] C. E. Max, C. F. McKee, and W. C. Mead, Phys. Fluids **23**, 1620 (1980).
[2] T. J. Goldsack, J. D. S. Kilkenny, B. J. MacGowan, P. F. Cunningham, C. L. S. Lewis, M. H. Key, and P. T. Rumsby, Phys. Fluids **25**, 1634 (1982).
[3] B. Yaakobi, J. Delettrez, L. M. Goldman, R. L. McCrory, R. Marjoribanks, M. C. Richardson, D. Shvartz, S. Skupsky, J. M. Soores, C. Verdon, D. M. Villeneuve, T. Boehly, R. Hutchison, and S. Letzring, Phys. Fluids **27**, 516 (1984).
[4] B. Yaakobi, T. Boehly, P. Bourke, Y. Conturie, R. S. Craxton, J. Delettrez, J. M. Forsyth, R. D. Frankel, L. M. Goldman, R. L. McCrory, M. C. Richardson, W. Seka, D. Shvarts, and J. M. Soures, Optics Commun. **39**, 175 (1981).
[5] A. R. Bell, R. G. Evans, and D. J. Nicholas, Phys. Rev. Lett. **46**, 247 (1981).
[6] J. Soures, R. J. Hutchinson, S. D. Jacobs, L. D. Lund, R. L. McCrory, and M. C. Richardson, in *Proceedings of the 10th Symposium on Fusion Engineering, December 1983, Philadelphia, PA* (IEEE, New York, 1984), p. 1392.
[7] R. S. Craxton, Optics Commun. **34**, 474 (1980); W. Seka, S. D. Jacobs, J. E. Rizzo, R. Boni, and R. S. Craxton, Optics Commun. **34**, 469 (1980).
[8] Earlier versions of LILAC are described in Laboratory for Laser Energetics Reports No. 16 (1973) and No. 36 (1976); opacity tables from W. F. Huebner, A. L. Merts, N. H. Magee, and M. F. Argo, Los Alamos Report No. LA-6760 (1977).
[9] W. Seka, J. M. Soures, S. D. Jacobs, L. D. Lund, and R. S. Craxton, IEEE J. Quantum Electron. **QE-17**, 1689 (1981).
[10] M. C. Richardson, R. S. Marjoribanks, S. A. Letzring, J. M. Forsyth, and D. M. Villeneuve, IEEE Journal of Quant. Electron. **QE-19**, 1861 (1983).
[11] M. C. Richardson, R. S. Craxton, J. Delettrez, R. Keck, R. L. McCrory, W. Seka, and J. M. Soures (unpublished).
[12] J. A. Tarvin, W. B. Fechner, J. T. Larsen, P. D. Rockett, and D. C. Slater, Phys. Rev. Lett. **51**, 1355 (1983).